Computational Investigation of Fibrin Mechanical and Damage Properties at the Interface Between Native Cartilage and Implant

Ali Vahdati

Yang Zhao

Timothy C. Ovaert

Diane R. Wagner[1]
e-mail: dwagner@nd.edu

Bioengineering Graduate Program,
Aerospace and Mechanical
Engineering Department,
University of Notre Dame,
Notre Dame, IN 46556

Scaffold-based tissue-engineered constructs as well as cell-free implants offer promising solutions to focal cartilage lesions. However, adequate mechanical stability of these implants in the lesion is required for successful repair. Fibrin is the most common clinically available adhesive for cartilage implant fixation, but fixation quality using fibrin is not well understood. The objectives of this study were to investigate the conditions leading to damage in the fibrin adhesive and to determine which adhesive properties are important in preventing delamination at the interface. An idealized finite element model of the medial compartment of the knee was created, including a circular defect and an osteochondral implant. Damage and failure of fibrin at the interface was represented by a cohesive zone model with coefficients determined from an inverse finite element method and previously published experimental data. Our results demonstrated that fibrin glue alone may not be strong enough to withstand physiologic loads in vivo while fibrin glue combined with chondrocytes more effectively prevents damage at the interface. The results of this study suggest that fibrin fails mainly in shear during off-axis loading and that adhesive materials that are stronger or more compliant than fibrin may be good alternatives due to decreased failure at the interface. The present model may be used to improve design and testing protocols of bioadhesives and give insight into the failure mechanisms of cartilage implant fixation in the knee joint.
[DOI: 10.1115/1.4007748]

Keywords: cartilage implant, fibrin, finite element model, chondral defect, articular cartilage repair, cohesive zone model

1 Introduction

Focal cartilage lesions of the knee affect approximately 900 000 individuals in the United States alone each year [1]. Due to the avascular nature and low cell-matrix ratio of articular cartilage (AC), these lesions are usually irreversible. In addition to activity-specific pain associated with them, AC lesions can also lead to osteoarthritis if they remain untreated [2, 3]. Current treatments for cartilage lesions less than 2 cm^2 include microfracture, autologous osteochondral transplantation, and autologous chondrocyte implantation (ACI). However, these techniques suffer from limitations, such as the amount of material available, insufficient formation of hyaline cartilage, donor site morbidity, lack of durability, and inability to integrate at the cartilage interface [4]. As an alternative, implanted cartilage replacements (ICRs) that fill the focal defect have been investigated. The ICRs under development include both cell-seeded, scaffold-based tissue-engineered constructs as well as cell-free implants that may be made of hydrogels, such as poly(vinyl alcohol) [5–8].

Adequate mechanical stability of the ICR in the lesion is required for successful cartilage repair [9, 10]. ICR adhesion to the native AC should be secure enough that it withstands the postoperative deformations and forces during joint movement. Adequate fixation ensures that the two surfaces are in apposition to one another and may allow integrative tissue to form. A completely delaminated ICR can cause unsatisfactory clinical results due to the introduction of the loose body in the joint space; consequently locking the knee [9, 11].

Although fibrin is the most common clinically available adhesive for ICR fixation in small symptomatic chondral defects, the fixation quality is not well understood. In a recent clinical study of matrix-induced ACI, fibrin glue partially or completely failed in two of 16 patients at an early stage [12].

We previously created a finite element (FE) model of a tissue-engineered osteochondral ICR in a focal cartilage defect in the knee joint and investigated the effects of implant material properties and integration at the interface on the mechanical environment of the ICR and the surrounding tissue [13]. We reported that inferior material properties and lack of integration alters the mechanical environment of both the implant and the native cartilage. However, delamination at the interface could not be explored because our model was limited to the cases of full integration or no integration at the interface. Additionally, our previous model was axisymmetric, which precluded the consideration of the relative sliding between the articular surfaces. Thus our objective here was to study damage in fibrin adhesive under conditions that mimic *in vivo* loading in the knee joint. We also conducted a sensitivity analysis to determine which adhesive properties are important in preventing delamination at the interface of an osteochondral implant and native AC.

2 Methods

2.1 Cohesive Zone Model of Fibrin Adhesive. Damage and failure of the fibrin adhesive was modeled utilizing the cohesive

[1]Corresponding author.
Contributed by the Bioengineering Division of ASME for publication in the JOURNAL OF BIOMECHANICAL ENGINEERING. Manuscript received March 28, 2012; final manuscript received September 19, 2012; accepted manuscript posted September 29, 2012; published online October 26, 2012. Editor: Victor H. Barocas.

zone modeling (CZM) technique with a bilinear traction-separation law (Fig. 1(*A*)) in commercial FE software ABAQUS 6.10 (Dassault Systèmes, RI, USA). The bilinear traction-separation law relates the maximum interfacial strength to the separation of two surfaces. In this triangular law, the material behavior of the adhesive is linear elastic until separation δ_{init} is reached. Beyond that, damage increases until separation reaches δ_{fail} and the adhesive fails (Fig. 1(*A*)). The area under the traction-separation curve represents the fracture energy. Modeling damage with the CZM technique in ABAQUS™ requires a damage initiation criterion and a damage evolution law. A maximum stress criterion for damage initiation and displacement-based damage evolution were adopted in this study. Compressive loads and strains do not cause damage in the cohesive zone in this model. As the default, fibrin properties in tension and shear were assumed to be the same.

Cohesive zone properties for both fibrin alone and fibrin combined with chondrocytes were determined from published experimental data of tensile tests to failure [14, 15]. Silverman et al. [14] applied fibrin glue with and without chondrocytes to the interfaces of pairs of cartilage discs and then implanted the constructs in subcutaneous pockets of nude mice. Constructs were harvested at 6 weeks and tensile tests were performed until the fibrin bond between the two cartilage discs failed. From the load-displacements curves, slope, tensile strength, failure displacement and failure energy of the constructs were calculated and reported [14]. To determine the cohesive zone properties for fibrin, we created FE models of cartilage-fibrin constructs (Fig. 1(*B*)) and simulated the tensile test performed by Silverman et al. [14]. Incompressible transversely isotropic mechanical properties were assigned to cartilage (for more detail on mechanical properties see Sec. 2.3). In Silverman et al.'s experiment, the flat ends of the constructs was attached to Plexiglass rods using cyanoacrylate. We applied this boundary condition by constraining displacements of the nodes on the flat ends of the constructs with respect to one another. Similar to the experimental setup, tensile displacement was applied to the constructs at a rate of 15 μm/s until complete failure was reached. Cohesive parameters for the fibrin, both with and without chondrocytes, were obtained with an inverse iterative finite element technique [16]. An optimization algorithm minimized the sum of the squared errors between the published cartilage-fibrin-cartilage experimental data and the model output. The data that were used in the optimization were the maximum tensile strength, the strain at initiation of damage, the failure energy and the ratio of failure displacement to displacement at damage initiation [14, 15]. The Pattern Search solver in the MATLAB™ (The MathWorks, Inc., Natick, MA) global optimization toolbox utilized a set of random start points to determine the global minimum of the objective function. Lower and upper bounds of cohesive zone properties were provided as constraints. The upper bounds were 1 MPa for modulus and tensile strength and 1 mm for displacement to failure. The lower bounds were set to 1×10^{-6} MPa for modulus and tensile strength and 1 μm for displacement to failure. The MATLAB™ optimization code consisted of an ensemble of subroutines that called a Python script, which in turn executed the ABAQUS™ model iteratively.

2.2 FE Model of the Medial Compartment of the Knee Joint. Idealized 3D models of intact tibial and femoral cartilage in the medial compartment of the human knee joint were constructed in SolidWorks 2010 (Dassault Systèmes, RI, USA) and were exported to ABAQUS 6.10 (Fig. 2). Incongruent joint surfaces in the model were given physiological radii of medial cartilage contact surfaces with different anterior-posterior and medial-lateral curvature [17]. In addition to the intact model, a model with a centrally-located 11 mm diameter tibial defect and an osteochondral ICR with curvature matching the tibia was constructed. Displacements of the nodes on the subchondral surface of the tibial and implanted cartilage were constrained in all directions, representing cartilage attachment to bone. Displacements of the nodes on the subchondral surface of the femoral cartilage were also constrained with respect to one another to allow for rigid body motion at this surface to simulate relative joint motion. A coefficient of friction of 0.02 was assigned for cartilage-cartilage contact, which is in the range of the experimental coefficient of friction reported for diarthrodial joints [18]. Geometric nonlinearity was accounted for using the NLGEOM option.

2.3 Cartilage and Implant Material Properties. It has been shown that the total stress in cartilage in an unconfined compression test at 0.2 s is only 0.14% different from that at time zero [19]. Considering the time duration of the normal gait cycle of approximately 1 s, and focusing our attention on terminal stance/preswing portion, the time duration for this analysis is close to 0.2 s and thus relatively short. Therefore, the effect of fluid flow was neglected and the material properties were represented by a single phase. Additionally, it has been shown that mechanical properties of a transversely isotropic biphasic material are equivalent to an incompressible transversely isotropic model for instantaneous loading of cartilage [20]. Thus in order to model the short-term response of cartilage to loading and to describe the effect of the collagenous network, incompressible transversely isotropic material properties [20] for native cartilage were

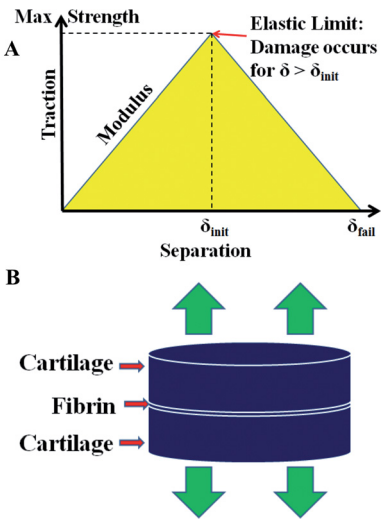

Fig. 1 (*A*) Schematic of bilinear traction-separation law and (*B*) model of fibrin-bonded cartilage discs in a tensile test

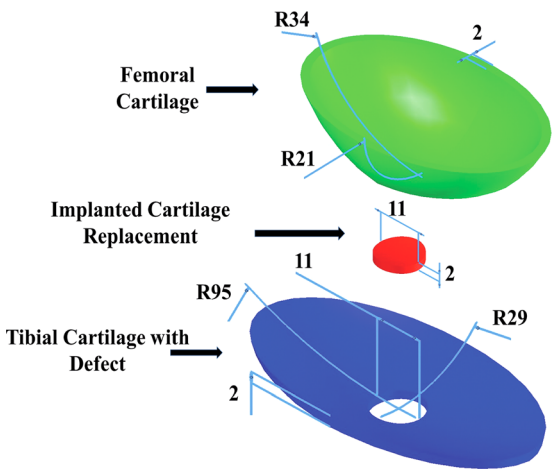

Fig. 2 Idealized model of the medial compartment of the knee joint with a circular defect and ICR. All dimensions are in mm.

Table 1 Average experimental data (± SD) [14, 15] and FE simulation results of tensile testing of fibrin-bonded cartilage discs

	Fibrin glue		Fibrin glue with cells	
	Experimental data	Simulation results	Experimental data	Simulation results
Slope of the stress-strain curve (MPa)	0.21 ± 0.07[a]	0.27	0.74 ± 0.22[a]	0.55
Tensile strength (MPa)	$9.9 \times 10^{-3} \pm 9.7 \times 10^{-3}$[a]	11×10^{-3}	0.065 ± 0.024[a]	0.066
Initiation of damage strain (%)	$0.04 \pm 2.6 \times 10^{-2}$[a]	0.04	0.17 ± 0.061[a]	0.12
Failure energy (J)	$3.1 \times 10^{-5} \pm 5.4 \times 10^{-5}$[a]	2.6×10^{-5}	$4.9 \times 10^{-4} \pm 3.2 \times 10^{-4}$[a]	4.0×10^{-4}
Displacement to failure/displacement to damage initiation	1.4 ± 0.66[b]	1.4	N/A	N/A

[a]Reference [14].
[b]Reference [15].

assigned: $E_{11} = 3.3$ MPa, $E_{33} = 6.2$ MPa, $\nu_{31} = 0.49$, $\nu_{23} = 1\text{-}0.5(E_{33}/E_{11})$, and $G_{23} = 7.5$ MPa, where the 1-direction is perpendicular to the cartilage surface at every element, and the 2- and 3-directions are parallel to the surface and perpendicular to each other. Properties in the 2- and 3-directions were symmetric. ICRs normally lack organized collagen fibers and are sufficiently modeled as isotropic [21]. The ICR was assigned a Young's modulus of 3.3 MPa, equal to the through-thickness stiffness of the native AC, and a Poisson ratio of 0.3. It has been suggested that the collagen network plays an important role in governing the instantaneous Poisson ratio of cartilage [22]. While the native AC was modeled as nearly incompressible, the ICR was assigned a lower Poisson's ratio due to the fact that similar to immature cartilage, most tissue-engineered constructs lack an organized collagen fiber distribution and have a lower collagen content and cross-link density compared to native AC [22].

2.4 Loading Conditions. Loading simulated the terminal stance/preswing phase of gait. During this portion of the gait cycle, cartilage deformation and the posterior-anterior excursion are the greatest and both contact area and cartilage deformation are nearly constant [23]. Thus, this portion of the stance phase of gait includes the maximum loading conditions and maximum relative motion and may be approximated by a simple posterior-anterior sliding motion of the femur over the tibia. A centrally-located axial compressive load was ramped linearly from 0 to 170 N in the y-direction (Fig. 2). Then, to mimic the posterior-anterior excursion of the femur over the tibia during the terminal stance/preswing phase of gait, the femur slid 5 mm across the tibia [23] by rotating the femur around the center of anterior-posterior curvature of the tibia while the load was kept constant and the load vector followed the rotation of the femoral condyle.

2.5 Validation and Parametric Study. To validate the FE model of the idealized knee compartment, results from the model with intact tibial cartilage (without the implant) were compared to clinical data of the maximum cartilage deformation and contact area at the terminal stance/preswing phase of gait [23, 24].

The cohesive zone model was utilized at the interface between the ICR and native AC in the knee model to investigate the effect of different adhesive properties on the failure of fixation. Fixation failure was visualized with color maps of the scalar damage variable, D. The bilinear traction-separation law defines degradation of stiffness as the evolution (between initiation and complete failure) of the damage variable, D, which is a function of the effective separation beyond damage initiation. $D = 0$ implies that the damage initiation criteria has not been met while $D = 1$ means that the maximum degradation value has been reached, the material has lost its load-carrying capacity, and that the adhesive has completely failed. First we compared the adhesive damage in the model with fibrin glue alone to the model with fibrin glue containing chondrocytes. Next, the evolution of damage in the fibrin alone was studied during different phases of loading. Finally, in order to investigate the effect of different adhesive properties on fixation failure, the fibrin strength was doubled in tension, shear or both; the modulus was decreased by 50% in tension, shear or both and finally δ_{fail} - δ_{init} (in terms of total displacement) was increased incrementally by 100% and 200%.

The model of fibrin-bonded cartilage discs used to determine adhesive properties from experimental data consisted of 600 axisymmetric CAX4R elements. The intact joint model and the model with implant consisted of 66 262 and 228 504 linear tetrahedral elements of type C3D4, respectively. Mesh sensitivity analysis was performed to make sure the results were not significantly affected with further mesh refinement.

3 Results

Good agreement between the simulation of the cartilage-fibrin tensile test and experimental results was reached (Table 1). In the simulations, fibrin glue containing chondrocytes demonstrated higher maximum strength, modulus, failure displacement, and fracture energy compared to fibrin glue alone after 6 weeks of *in vivo* culture (Table 2, Fig. 3(*A*)). In the simulated tensile tests, fibrin glue alone withstood a maximum load of 0.01 MPa while fibrin glue with chondrocytes resisted a much higher maximum load of 0.07 MPa (Fig. 3(*B*)), closely matching the experimental data.

In the simulated intact model without the implant, axial deformation at the center of contact was 20% of the total cartilage thickness and the contact area was 260 mm^2. The maximum deformation and contact area obtained from the present study fell well within the ranges of experimental measurements [24–27]. Contact area increased gradually during axial loading and then remained relatively constant during sliding (Fig. 4(*C*)). This relatively constant contact area and cartilage deformation (data not shown) during sliding approximated the terminal stance/preswing phase of gait [23].

A comparison of the distribution pattern of contact stress at the cartilage surface between the intact model and the model including the ICR showed some interesting differences. The contact stress distribution was noticeably altered when the ICR was introduced in the model (Figs. 4(*A*) and 4(*B*)). While the intact joint showed a peak contact stress at the center of the contact, the joint with the implanted ICR showed a contact stress concentration in native cartilage in the vicinity of defect rim after axial loading (Figs. 4(*A*) and 4(*B*)). This contact stress concentration was accompanied by a decrease in contact stress in the ICR.

Table 2 Cohesive zone properties used to model fibrin

	Fibrin glue	Fibrin glue with cells
Modulus (MPa)	0.106	0.250
Tensile strength (MPa)	0.012	0.076
Displacement to failure (mm)	0.022	0.072

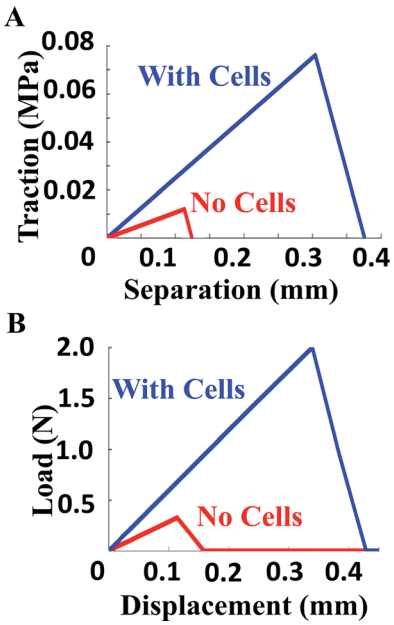

Fig. 3 (*A*) Bilinear traction-separation CZM law for fibrin adhesive. Red and blue lines represent fibrin without and with cells, respectively. (*B*) Computational load-displacement response of cartilage-fibrin constructs in tension.

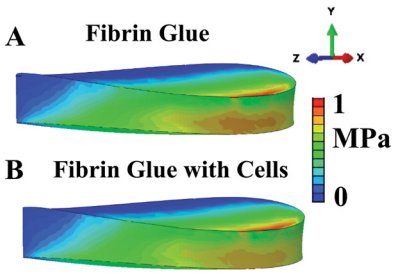

Fig. 5 (*A*) Maximum shear stress distribution in the ICR when fibrin glue alone or (*B*) fibrin glue with chondrocytes is used as the adhesive material.

From the time-history of damage dissipation energy in the fibrin alone, it can be seen that the fibrin does not fail during initial axial loading (Fig. 4(*D*)). During sliding, damage starts to develop in the fibrin and damage dissipation energy reaches a maximum value of 8.1 μJ at the end of sliding (Fig. 4(*D*)). While fibrin glue containing chondrocytes after 6 weeks of *in vivo* culture prevented damage in the adhesive layer completely (data not shown), approximately 17% of the fibrin glue was damaged when used alone. An increased maximum shear stress on the ICR surface in the lower portion of the interface was observed when fibrin alone was used (Fig. 5(*A*)) as compared to when fibrin glue did not fail (i.e., when fibrin glue with chondrocytes was used as adhesive material) (Fig. 5(*B*)).

Next, the effect of increasing the adhesive strength and decreasing the adhesive modulus was studied (Fig. 6). While doubling the adhesive strength of fibrin in tension caused no decrease in the damaged area of the adhesive, doubling the shear strength resulted in complete lack of fibrin damage. Doubling both the shear and tensile strength of fibrin also prevented the formation of any damage at the interface. Reducing the adhesive modulus by a factor of 2 had a similar effect to doubling the strength and similarly demonstrated the importance of shear as opposed to tensile properties (Fig. 6).

Increasing $\Delta = \delta_{fail} - \delta_{init}$ by factors of 2 and 3 resulted in decreased fibrin damage (Fig. 7(*A*)), which was reflected in the damage dissipation energy (Fig. 7(*B*)). Damage dissipation energy for fibrin glue decreased by 18% and 44% when Δ was increased by factors of 2 and 3, respectively. While damage level and damage dissipation energy decreased with increasing Δ, damaged fibrin area remained relatively constant (Fig. 7(*C*)).

4 Discussion

One of the major concerns for a surgeon performing scaffold-based cartilage repair is the secure retention of the ICR at the desired position in the knee joint [28]. In order to keep the ICR stable in the defect area, one strategy would be to take advantage of the healing ability of bone to anchor an osteochondral plug consisting of distinct cartilaginous and bony layers [28]. Although osteochondral grafts are stabilized by integration with the subchondral bone, integration with the cartilage remains a problem. The intrinsic antiadhesiveness of cartilage, due to its low friction surfaces and high proteoglycan content, make it even more difficult for the implant to integrate with the host tissue [29]. In order to solve this problem, fibrin glue is commonly used for fixation of ICRs in the defect. Many new cartilage repair techniques which are currently in clinical trials, such as Biocart II (ProChon Biotech Ltd, Rehovot, Israel), cartilage autograft implantation system (CAIS, Depuy-Mitek, Raynham, MA), DeNovo engineered tissue (Zimmer Inc.), and matrix induced autologous chondrocyte

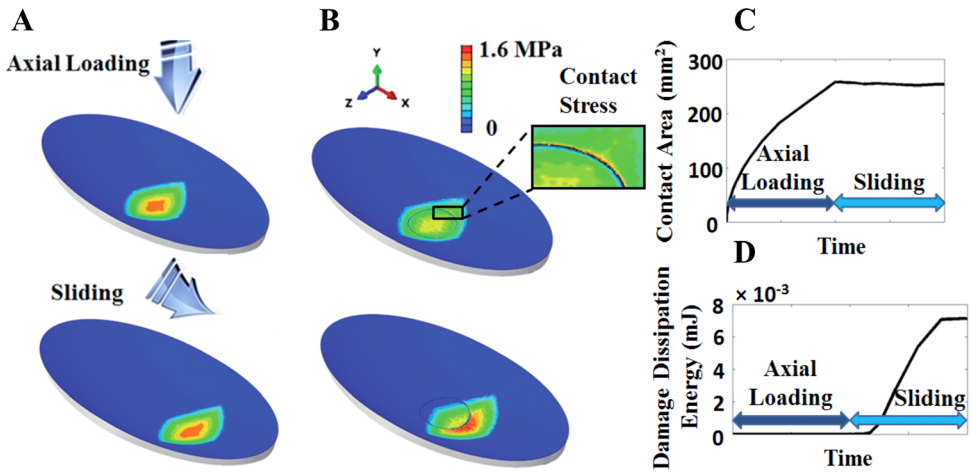

Fig. 4 Surface contact stress distribution after axial and sliding loading for (*A*) intact model and (*B*) model with ICR. Time history of (*C*) contact area in the intact case and (*D*) of damage dissipation energy in the model with the ICR.

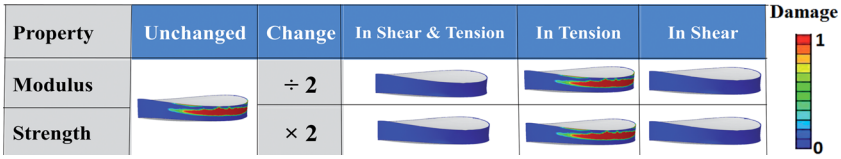

Fig. 6 Effect of changing fibrin strength and modulus on damage formation

implantation (MACI, Genzyme Europe, Naarden, Netherlands) use fibrin for implant fixation.

While delamination of cartilage implants occurs mainly in the first six months after the operation [30], experimental evaluation of postoperative implant stability is difficult. Mechanical failure of the adhesive between the cartilage implant and surrounding cartilage is a relatively unexplored field of orthopedic biomechanics and only a few in vitro and ex vivo experiments are reported in the literature. Drobnic et al. [10] reported the first analysis of the stability of primary fixation for tissue-engineered cartilage grafts. They investigated different fixation techniques including fibrin glue for collagen scaffolds in a cadaveric study with continuous passive motion of the knee joint to simulate the initial postoperative period of rehabilitation. In this study, scaffolds fixed with fibrin glue showed insufficient fixation quality and detached from the lesion under loading. Applying uniaxial tensile testing in an open side defect, Knecht et al. [9] tested the fixation quality of several synthetic ICRs with four different fixation techniques: unfixed, fibrin glue, chondral suture, and transosseous suture. This group reported that fibrin glue fixation did not provide the same degree of scaffold attachment to the surrounding cartilage as was provided by the sutures regardless of the scaffold type. Bekkers et al. [31] applied a force perpendicular to the scaffold surface in a human cadaver knee model. In this study, fibrin glue provided a weak attachment when compared to the suturing techniques. Efe et al. [32] established an ex vivo animal model in order to assess the primary stability of cell-free collagen gel plugs. The same group recently showed that press-fit only and press-fit combined with fibrin glue both provided similar mechanical stability and thus adding fibrin glue to the lesions did not improve graft fixation in the porcine continuous passive motion model [33]. None of the above-mentioned experimental protocols fully simulated *in vivo* knee joint loads and activity-specific motion of the joint, since no force was applied by the muscles. Thus due to limitations in such controlled experimental studies, transferring these in vitro and ex vivo results to the *in vivo* situation can be difficult.

The underlying motivation for this study was to develop a computational tool that could be used to identify variables important in the design and/or selection of adhesives for ICR fixation. The key findings from the study were that (1) fibrin glue alone may not be strong enough to withstand physiological loads *in vivo*. On the other hand, fibrin glue combined with cells significantly limits the damage at the interface after 6 weeks. However, the simplifications in the model, particularly with regards to loading conditions and material properties, make it difficult to state definitely that damage would not occur *in vivo* with this stronger adhesive; (2) fibrin glue at the interface fails mainly in shear. Thus shear is the most appropriate test for any adhesive developed for ICR fixation prior to *in vivo* application in order to ensure adequate fixation strength; (3) adhesive materials that are stronger or are more compliant may decrease failure at the interface and thus can be a good alternative to fibrin glue. One strategy for improving and "tuning" fibrin's mechanical properties is crosslinking fibrin with another chemical agent. This strategy was utilized to develop genipin-crosslinked fibrin for cartilage tissue engineering [34] and the repair of the annulus fibrosus in the intervertebral disc [35]. Other solutions could include new adhesives such as a recently reported chondroitin sulfate bioadhesive, which showed a strength of ~46 kPa in both tension and shear [36].

There is a wide range of experimental data on the strength of fibrin when joining biological tissues in different experimental protocols: 4.5 kPa in uniaxial tension with rat skin [37], 13.3 kPa in a blister test with pig skin dermal grafts [16], 0.7 kPa in a lap shear test with porcine skin [38], 8 kPa in a lap shear test with human saphenous vein [39], 23.2 kPa in shear at the periosteum–cartilage interface [40], and approximately 17 kPa in shear at the cartilage-cartilage interface after 5 min of incubation [29]. Thus the cohesive strength of 12 kPa for fibrin glue in the present study falls well within the range of available experimental data. The cohesive strength of fibrin glue with chondrocytes in our study was substantially larger at 76 kPa.

The time history plot of damage dissipation energy (Fig. 4(*D*)) demonstrates that fibrin adhesive is damaged during the sliding phase of loading and reaches maximum damage at the end of travel. Fibrin failure is likely due to the off-axis loading applied to the implant, which also increases during sliding in our model. As relative joint motion is typical during walking and most other

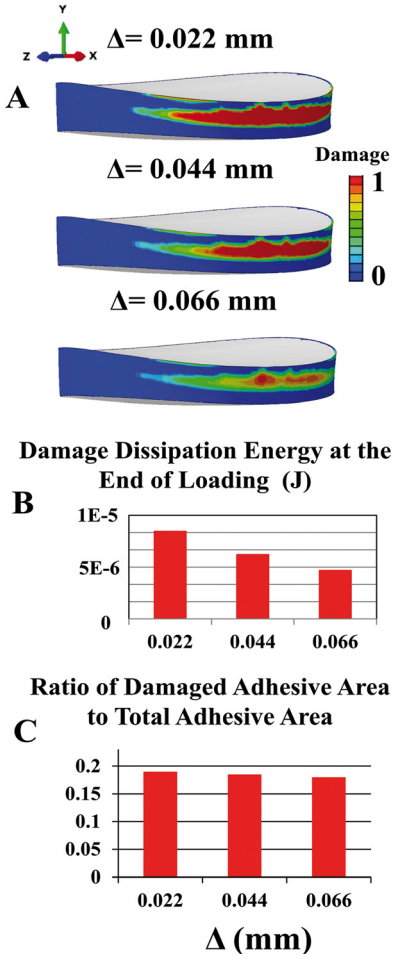

Fig. 7 (*A*) Effect of increasing $\Delta = \delta_{fail} - \delta_{init}$ on damage level in the adhesive, (*B*) damage dissipation energy at the end of loading, and (*C*) ratio of damaged adhesive area to total adhesive area

daily activities, it is likely that ICRs *in vivo* would be regularly subjected to these off-axis loads. Thus our results demonstrate the importance of approximating physiological loading conditions in simulations and experiments designed to understand failure of ICR fixation.

The damage in our simulation was mostly localized to the top half of the interface; the lower half did not show any damage (Fig. 5(*A*)). This result is similar to the pattern of fibrin failure observed in the ex vivo study of Drobnic et al. [10]. There was no damage when the adhesive properties were either stronger or more compliant than fibrin in shear. Conversely, when the adhesive was stronger or more compliant in tension, no reduction in adhesive damage was observed (Fig. 6). From these results, we conclude that shear displacements at the interface are the main mechanism of ICR delamination *in vivo*, because it is the shear properties that determine whether or not the adhesive fails, while the tensile properties have no such effect. Thus adhesives that are stronger and/or more compliant than fibrin under shear loading could prevent failure of ICR fixation in the knee joint. Increasing $\Delta = \delta_{\text{fail}} - \delta_{\text{init}}$ by factors of 2 and 3 resulted in decreases in the damage level as expected. An increase in Δ increases the area under traction-separation curve and results in higher adhesive fracture energy. Changing the value of Δ only affects the propagation of damage and does not change the damage initiation (Fig. 1(*B*)). Thus while a larger Δ resulted in decreased damaged levels, the damaged area was not affected (Fig. 7(*C*)).

Compared to the response of fibrin with chondrocytes after six weeks of implantation, our results showed that fibrin alone can result in increased shear stress on the lower half of the implant surface (Fig. 5), which did not delaminate. It is hard to say whether the higher shear stress in the case of fibrin alone is due to the fibrin failure in the upper portion of the interface, or due to different material properties compared to fibrin combined with chondrocytes. Nonetheless, this increased shear stress could lead to an altered cellular response for either native cells or cell-seeded scaffolds and may be detrimental to the structural integrity of the implant. Increased shear stress could also lead to accelerated damage under additional loading cycles.

A number of simplifications in modeling the knee joint and materials were made. One simplification in the present study was the use of an idealized knee anatomy. However, cartilage deformation and area of contact for the articular surfaces compared well with experimental data from the literature. Thus we believe that the predictions reported in this study are valid in an indicative sense. Another simplification in regards to modeling cartilage material was that depth-dependent material properties and tension-compression nonlinearity [41,42] were not included in the constitutive model. In a preliminary study, we modeled the superficial zone as transversely isotropic with higher tensile stiffness in the directions parallel to the surface while the middle and deep zones were modeled as isotropic. Although this modeling approach was computationally more expensive than a fully transversely isotropic model, it did not affect the results significantly. Additionally, under the loading regime in the current study, the material properties in the compressive direction are different from those tangential to the surface, which experiences tension in the superficial zone [43]. Therefore, due to the transversely isotropic material properties, the addition of tension/compression nonlinearity to the model would only have a minor effect on the results. Accurately representing the depth-dependent variations in mechanical properties may require a more complex approach such as including the arcade-shaped distribution of collagen fibers and depth-dependent distribution of proteoglycans. There have been very few three-dimensional computer models that include effect of collagen fiber distribution through the depth of cartilage [44,45] and perhaps due to their computational expense, these models only included axial loading without looking at the effect of sliding.

On average, a person takes $1–2 \times 10^6$ steps per year [46], thus the mechanical environment experienced by the adhesive at the interface would be more severe than the single loading condition simulated here. Since the AC in the knee is subjected to a wide variety of static and dynamic loading conditions [47], it will be useful to study the effect of more complex and long-term loading conditions, such as cyclic loading and impact on the fixation of ICRs.

Fibrin glue failure was modeled by a cohesive process zone, in which all inelastic phenomena were accumulated and mathematically captured by a bilinear traction-separation law. This simplification ignores time-dependent properties, dissipative phenomena and nonlinearity in fibrin glue. Nonetheless, bilinear traction-separation laws have been recently applied to model the failure of soft biological tissue. Forsell and Gasser [48] performed a FE simulation of failure of ventricular tissue due to deep penetration utilizing a bilinear traction-separation law. In this study, dissipative effects and material nonlinearity had a minor impact on the simulation results. Additionally, experimental data shows that the mechanical behavior of fibrin is dominated by elastic rather than viscoplastic behavior [15, 49]. For this reason, the viscoelasticity of fibrin was assumed to be negligible in our study.

Results from these FE models provide an important understanding of the failure of fibrin fixation and consequently the integration of implants that repair focal cartilage defects. Inadequate fixation quality of fibrin glue when used alone, mechanism of the failure of fibrin at the interface due to shear deformations and insight into methods to improve the mechanical properties of fibrin were demonstrated by this computational study. The present model may be applied to evaluate other factors in scaffold fixation for cartilage repair; additional studies are planned that will investigate the effect of ICR size, location, material properties, and full versus partial thickness chondral defects on the failure of the adhesive at the interface. In the future, this model may be used to improve design and testing protocols of bioadhesives and give insight into the failure mechanisms of ICR fixation in the knee joint.

References

[1] Minas, T., and Nehrer, S., 1997, "Current Concepts in the Treatment of Articular Cartilage Defects," Orthopedics, **20**(6), pp. 525–538.

[2] Cicuttini, F., Ding, C., Wluka, A., Davis, S., Ebeling, P. R., and Jones, G., 2005, "Association of Cartilage Defects With Loss of Knee Cartilage in Healthy, Middle-Age Adults: A Prospective Study," Arthritis. Rheum., **52**(7), pp. 2033–2039.

[3] Ding, C., Garnero, P., Cicuttini, F., Scott, F., Cooley, H., and Jones, G., 2005, "Knee Cartilage Defects: Association With Early Radiographic Osteoarthritis, Decreased Cartilage Volume, Increased Joint Surface Area and Type II Collagen Breakdown," Osteoarthritis Cartilage, **13**(3), pp. 198–205.

[4] Martin, I., Miot, S., Barbero, A., Jakob, M., and Wendt, D., 2007, "Osteochondral Tissue Engineering," J. Biomech., **40**(4), pp. 750–765.

[5] Maher, S. A., Doty, S. B., Torzilli, P. A., Thornton, S., Lowman, A. M., Thomas, J. D., Warren, R., Wright, T. M., and Myers, E., 2007, "Nondegradable Hydrogels for the Treatment of Focal Cartilage Defects," J. Biomed. Mater. Res. Part A, **83A**(1), pp. 145–155.

[6] Thomas, B. H., Craig Fryman, J., Liu, K., and Mason, J., 2009, "Hydrophilic-Hydrophobic Hydrogels for Cartilage Replacement," J. Mech. Behav. Biomed., **2**(6), pp. 588–595.

[7] Coutts, R. D., Healey, R. M., Ostrander, R., Sah, R. L., Goomer, R., and Amiel, D., 2001, "Matrices for Cartilage Repair," Clin. Orthop. Relat. Res., Suppl. **391**, pp. S271–S279.

[8] Ahmed, T. A., and Hincke, M. T., 2010, "Strategies for Articular Cartilage Lesion Repair and Functional Restoration," Tissue Eng. Part B, Rev., **16**(3), pp. 305–329.

[9] Knecht, S., Erggelet, C., Endres, M., Sittinger, M., Kaps, C., and Stussi, E., 2007, "Mechanical Testing of Fixation Techniques for Scaffold-Based Tissue-Engineered Grafts," J. Biomed. Mater. Res. B, **83**(1), pp. 50–57.

[10] Drobnic, M., Radosavljevic, D., Ravnik, D., Pavlovcic, V., and Hribernik, M., 2006, "Comparison of Four Techniques for the Fixation of a Collagen Scaffold in the Human Cadaveric Knee," Osteoarthritis Cartilage, **14**(4), pp. 337–344.

[11] Nehrer, S., Spector, M., and Minas, T., 1999, "Histologic Analysis of Tissue After Failed Cartilage Repair Procedures," Clin. Orthop. Relat. Res., **365**, pp. 149–162.

[12] Marlovits, S., Striessnig, G., Kutscha-Lissberg, F., Resinger, C., Aldrian, S. M., Vecsei, V., and Trattnig, S., 2005, "Early Postoperative Adherence of Matrix-Induced Autologous Chondrocyte Implantation for the Treatment of Full-Thickness Cartilage Defects of the Femoral Condyle," Knee Surg. Sports Traumatol. Arthrosc., **13**(6), pp. 451–457.

[13] Vahdati, A., and Wagner, D. R., 2011, "Finite Element Study of a Tissue-Engineered Cartilage Transplant in Human Tibiofemoral Joint," Comput. Methods Biomech. Biomed. Eng., (online).

[14] Silverman, R. P., Bonasser, L., Passaretti, D., Randolph, M. A., and Yaremchuk, M. J., 2000, "Adhesion of Tissue-Engineered Cartilage to Native Cartilage," Plast. Reconstr. Surg., **105**(4), pp. 1393–1398.
[15] Sierra, D. H., Eberhardt, A. W., and Lemons, J. E., 2002, "Failure Characteristics of Multiple-Component Fibrin-Based Adhesives," J. Biomed. Mater. Res., **59**(1), pp. 1–11.
[16] Liu, K., Van Landingham, M. R., and Ovaert, T. C., 2009, "Mechanical Characterization of Soft Viscoelastic Gels via Indentation and Optimization-Based Inverse Finite Element Analysis," J. Mech. Behav. Biomed. Mater., **2**(4), pp. 355–363.
[17] Koo, S., and Andriacchi, T. P., 2007, "A Comparison of the Influence of Global Functional Loads Vs. Local Contact Anatomy on Articular Cartilage Thickness at the Knee," J. Biomech., **40**(13), pp. 2961–2966.
[18] Mow, V. C., Ateshian, G. A., and Spilker, R. L., 1993, "Biomechanics of Diarthrodial Joints: A Review of Twenty Years of Progress," J. Biomech. Eng., **115**(4B), pp. 460–467.
[19] Eberhardt, A. W., Keer, L. M., Lewis, J. L., and Vithoontien, V., 1990, "An Analytical Model of Joint Contact," J. Biomech. Eng., **112**(4), p. 407.
[20] Garcia, J. J., Altiero, N. J., and Haut, R. C., 1998, "An Approach for the Stress Analysis of Transversely Isotropic Biphasic Cartilage Under Impact Load," J. Biomech. Eng., **120**(5), pp. 608–613.
[21] Kelly, D. J., and Prendergast, P. J., 2006, "Prediction of the Optimal Mechanical Properties for a Scaffold used in Osteochondral Defect Repair," Tissue Eng., **12**(9), pp. 2509–2519.
[22] Wong, M., Ponticiello, M., Kovanen, V., and Jurvelin, J. S., 2000, "Volumetric Changes of Articular Cartilage During Stress Relaxation in Unconfined Compression," J. Biomech., **33**(9), pp. 1049–1054.
[23] Liu, F., Kozanek, M., Hosseini, A., Van de Velde, S. K., Gill, T. J., Rubash, H. E., and Li, G., 2010, "*In Vivo* Tibiofemoral Cartilage Deformation during the Stance Phase of Gait," J. Biomech., **43**(4), pp. 658–665.
[24] Hosseini, A., Van de Velde, S. K., Kozanek, M., Gill, T. J., Grodzinsky, A. J., Rubash, H. E., and Li, G., 2010, "*In-Vivo* Time-Dependent Articular Cartilage Contact Behavior of the Tibiofemoral Joint," Osteoarthritis Cartilage, **18**(7), pp. 909–916.
[25] Paci, J. M., Scuderi, M. G., Werner, F. W., Sutton, L. G., Rosenbaum, P. F., and Cannizzaro, J. P., 2009, "Knee Medial Compartment Contact Pressure Increases With Release of the Type I Anterior Intermeniscal Ligament," Am. J. Sports Med., **37**(7), pp. 1412–1416.
[26] Patel, V. V., Hall, K., Ries, M., Lotz, J., Ozhinsky, E., Lindsey, C., Lu, Y., and Majumdar, S., 2004, "A Three-Dimensional MRI Analysis of Knee Kinematics," J. Orthop. Res., **22**(2), pp. 283–292.
[27] Bingham, J. T., Papannagari, R., Van de Velde, S. K., Gross, C., Gill, T. J., Felson, D. T., Rubash, H. E., and Li, G., 2008, "*In Vivo* Cartilage Contact Deformation in the Healthy Human Tibiofemoral Joint," Rheumatology, **47**(11), pp. 1622–1627.
[28] Martin, I., Miot, S., Barbero, A., Jakob, M., and Wendt, D., 2007, "Osteochondral Tissue Engineering," J. Biomech., **40**(4), pp. 750–765.
[29] Jurgensen, K., Aeschlimann, D., Cavin, V., Genge, M., and Hunziker, E. B., 1997, "A New Biological Glue for Cartilage-Cartilage Interfaces: Tissue Transglutaminase," J. Bone Jt. Surg., Am., **79**(2), pp. 185–193.
[30] Alparslan, L., Minas, T., and Winalski, C. S., 2001, "Magnetic Resonance Imaging of Autologous Chondrocyte Implantation," Semin. Ultrasound CT MR, **22**(4), pp. 341–351.
[31] Bekkers, J. E., Tsuchida, A. I., Malda, J., Creemers, L. B., Castelein, R. J., Saris, D. B., and Dhert, W. J., 2010, "Quality of Scaffold Fixation in a Human Cadaver Knee Model," Osteoarthritis Cartilage, **18**(2), pp. 266–272.
[32] Efe, T., Schofer, M. D., Fuglein, A., Timmesfeld, N., Fuchs-Winkelmann, S., Stein, T., El-Zayat, B. F., Paletta, J. R., and Heyse, T. J., 2010, "An Ex Vivo Continuous Passive Motion Model in a Porcine Knee for Assessing Primary Stability of Cell-Free Collagen Gel Plugs," BMC Musculoskelet. Disord., **11**, pp. 283–293.
[33] Efe, T., Fuglein, A., Heyse, T. J., Stein, T., Timmesfeld, N., Fuchs-Winkelmann, S., Schmitt, J., Paletta, J. R., and Schofer, M. D., 2012, "Fibrin Glue Does Not Improve the Fixation of Press-Fitted Cell-Free Collagen Gel Plugs in an Ex Vivo Cartilage Repair Model," Knee Surg. Sports Traumatol. Arthrosc., **20**(2), pp. 210–215.
[34] Dare, E. V., Griffith, M., Poitras, P., Kaupp, J. A., Waldman, S. D., Carlsson, D. J., Dervin, G., Mayoux, C., and Hincke, M. T., 2009, "Genipin Cross-Linked Fibrin Hydrogels for In Vitro Human Articular Cartilage Tissue-Engineered Regeneration," Cells Tissues Organs, **190**(6), pp. 313–325.
[35] Schek, R. M., Michalek, A. J., and Iatridis, J. C., 2011, "Genipin-Crosslinked Fibrin Hydrogels as a Potential Adhesive to Augment Intervertebral Disc Annulus Repair," Eur. Cells Mater., **21**, pp. 373–383.
[36] Wang, D. A., Varghese, S., Sharma, B., Strehin, I., Fermanian, S., Gorham, J., Fairbrother, D. H., Cascio, B., and Elisseeff, J. H., 2007, "Multifunctional Chondroitin Sulphate for Cartilage Tissue-Biomaterial Integration," Nature Mater., **6**(5), pp. 385–392.
[37] Alston, S. M., Solen, K. A., Broderick, A. H., Sukavaneshvar, S., and Mohammad, S. F., 2007, "New Method to Prepare Autologous Fibrin Glue on Demand," Transl. Res., **149**(4), pp. 187–195.
[38] McDermott, M. K., Chen, T., Williams, C. M., Markley, K. M., and Payne, G. F., 2004, "Mechanical Properties of Biomimetic Tissue Adhesive Based on the Microbial Transglutaminase-Catalyzed Crosslinking of Gelatin," Biomacromolecules, **5**(4), pp. 1270–1279.
[39] Kjaergard, H. K., Velada, J. L., Pedersen, J. H., Fleron, H., and Hollingsbee, D. A., 2000, "Comparative Kinetics of Polymerisation of Three Fibrin Sealants and Influence on Timing of Tissue Adhesion," Thromb. Res., **98**(2), pp. 221–228.
[40] Orr, T. E., Patel, A. M., Wong, B., Hatzigiannis, G. P., Minas, T., and Spector, M., 1999, "Attachment of Periosteal Grafts to Articular Cartilage With Fibrin Sealant," J. Biomed. Mater. Res., **44**(3), pp. 308–313.
[41] Ateshian, G. A., Rajan, V., Chahine, N. O., Canal, C. E., and Hung, C. T., 2009, "Modeling the Matrix of Articular Cartilage Using a Continuous Fiber Angular Distribution Predicts Many Observed Phenomena," J. Biomech. Eng., **131**(6), p. 061003.
[42] Wilson, W., van Donkelaar, C. C., van Rietbergen, B., and Huiskes, R., 2005, "A Fibril–Reinforced Poroviscoelastic Swelling Model for Articular Cartilage," J. Biomech., **38**(6), pp. 1195–1204.
[43] Owen, J. R., and Wayne, J. S., 2006, "Influence of a Superficial Tangential Zone Over Repairing Cartilage Defects: Implications for Tissue Engineering," Biomech. Model. Mechanobiol., **5**(2), pp. 102–110.
[44] Shirazi, R., and Shirazi-Adl, A., 2009, "Computational Biomechanics of Articular Cartilage of Human Knee Joint: Effect of Osteochondral Defects," J. Biomech., **42**, pp. 2458–2465.
[45] Li, L. P., Cheung, J. T., and Herzog, W., 2009, "Three-Dimensional Fibril-Reinforced Finite Element Model of Articular Cartilage," Med. Biol. Eng. Comput., **47**, pp. 607–615.
[46] Weightman, B., 1976, "Tensile Fatigue of Human Articular Cartilage," J. Biomech., **9**(4), pp. 193–200.
[47] Grodzinsky, A. J., Levenston, M. E., Jin, M., and Frank, E. H., 2000, "Cartilage Tissue Remodeling in Response to Mechanical Forces," Annu. Rev. Biomed. Eng., **2**, pp. 691–713.
[48] Forsell, C., and Gasser, T. C., 2011, "Numerical Simulation of the Failure of Ventricular Tissue Due to Deep Penetration: The Impact of Constitutive Properties," J. Biomech., **44**(1), pp. 45–51.
[49] Eyrich, D., Brandl, F., Appel, B., Wiese, H., Maier, G., Wenzel, M., Staudenmaier, R., Goepferich, A., and Blunk, T., 2007, "Long-Term Stable Fibrin Gels for Cartilage Engineering," Biomaterials, **28**(1), pp. 55–65.